Sensors & Actuators: B. Chemical 381 (2023) 133434

Contents lists available at ScienceDirect

Sensors and Actuators: B. Chemical

journal homepage: www.elsevier.com/locate/snb

STORM-based multi-functional carbon dots for investigating HS^- interaction with mitochondria in living cells

Jiaqing Guo [a,1], Jinying Wang [a,1], Aikun Liu [a,b], Hao Li [a,*], Yejun He [b], Junle Qu [a], Zhigang Yang [a,*], Jun Song [a,*]

[a] Center for Biomedical Optics and Photonics (CBOP) & College of Physics and Optoelectronic Engineering, Key Laboratory of Optoelectronic Devices and Systems, Shenzhen University, Shenzhen 518060, China
[b] College of Electronics and Information Engineering, Shenzhen University, Shenzhen 518060, PR China

ARTICLE INFO

Keywords:
STORM
P-CDs
Interaction
Higher resolution
Signal-to-background ratio

ABSTRACT

By investigating the interaction between subcellular components using visualization techniques, pathological processes can be intuitively analyzed to reveal the origins of associated disorders more efficiently. Based on the Stochastic optical reconstruction microscopy (STORM) imaging nanoscopy, this study is the first to achieve a higher resolution and high signal-to-background ratio image of living cells by employing photoblinking carbon dots (P-CDs). Accordingly, this example can be used to explore the interaction between subcellular structures more precisely and clearly. Thus, the current study provides a potent method for visualizing the etiology of associated disorders.

1. Introduction

With the advancement of the economy, technology, and related fields, people are paying greater attention to their personal health while also appreciating the material and spiritual aspects of life [1–4]. However, diseases affect not just human health, but also all elements of human existence; COVID-19 was a good example to demonstrate such aspect [5,6]. Therefore, a thorough understanding of the etiology of diseases will allow for the most effective treatment of the corresponding diseases, thereby maximizing human health [7,8]. The use of fluorescent probes to examine the interaction between various subcellular components in cells was one of the approaches to investigate the origins of diseases [9]. Typically, a fluorescent probe for examining the interaction of subcellular components must possess the following characteristics to be effective: Excellent photo-bleaching resistance [10], stable fluorescence properties [11], no bio-toxicity [12], excellent biocompatibility [13], good membrane permeability, and ease of manufacture [14,15].

In addition to the features above, fluorescent probes must target certain organelles and respond specifically to pH [16–19], ions [20–23], and molecules [24,25] in order to facilitate the study of specific biological problems [26–28]. The selection of appropriate fluorescent probes directly affects the observational effect of subcellular structure interaction. Accordingly, carbon dots (CDs) have been utilized as probes due to their high ions and molecule selectivity, as well as their superior ability to target organelles (nucleolus, lysosome, mitochondria) [29–31]. Correspondingly, CDs offer a wide range of applications for studying the interactions between organelles, ions, and molecules. For example, Gao employed p-phenylenediamine and thiourea to synthesize CDs that can not only target lysosomes but also quantitatively measure pH by fluorescence quenching. The CDs were then used to explore the interactions between lysosomes and pH in living cells [32]. In addition, Wang et al., developed a CD that could target the nucleolus and respond to pH and NO_2^- enabling the study of nucleolar physiological activities under fluorescence quenching at varying pH and NO_2^- concentrations [33]. Therefore, evident that the interaction between organelles and substances such as ions can be effectively studied by employing the specific targeting and response of CDs, which provides technical support for the visualization of the interaction of subcellular structures and the solution of corresponding biological problems.

Although observing the quenching of CDs fluorescence on targeted organelles enabled the study of the interaction of ions and other substances with cellular organelles, the signal-to-background ratio (SBR) in the cellular images decreases significantly as the response of ions and other substances to CDs increases and the fluorescence intensity (FI) of

* Corresponding authors.
E-mail addresses: lihao000000@163.com (H. Li), zhgyang@szu.edu.cn (Z. Yang), songjun@szu.edu.cn (J. Song).
[1] Jiaqing Guo and Jinying Wang contributed equally to this work.

https://doi.org/10.1016/j.snb.2023.133434
Received 15 November 2022; Received in revised form 22 January 2023; Accepted 25 January 2023

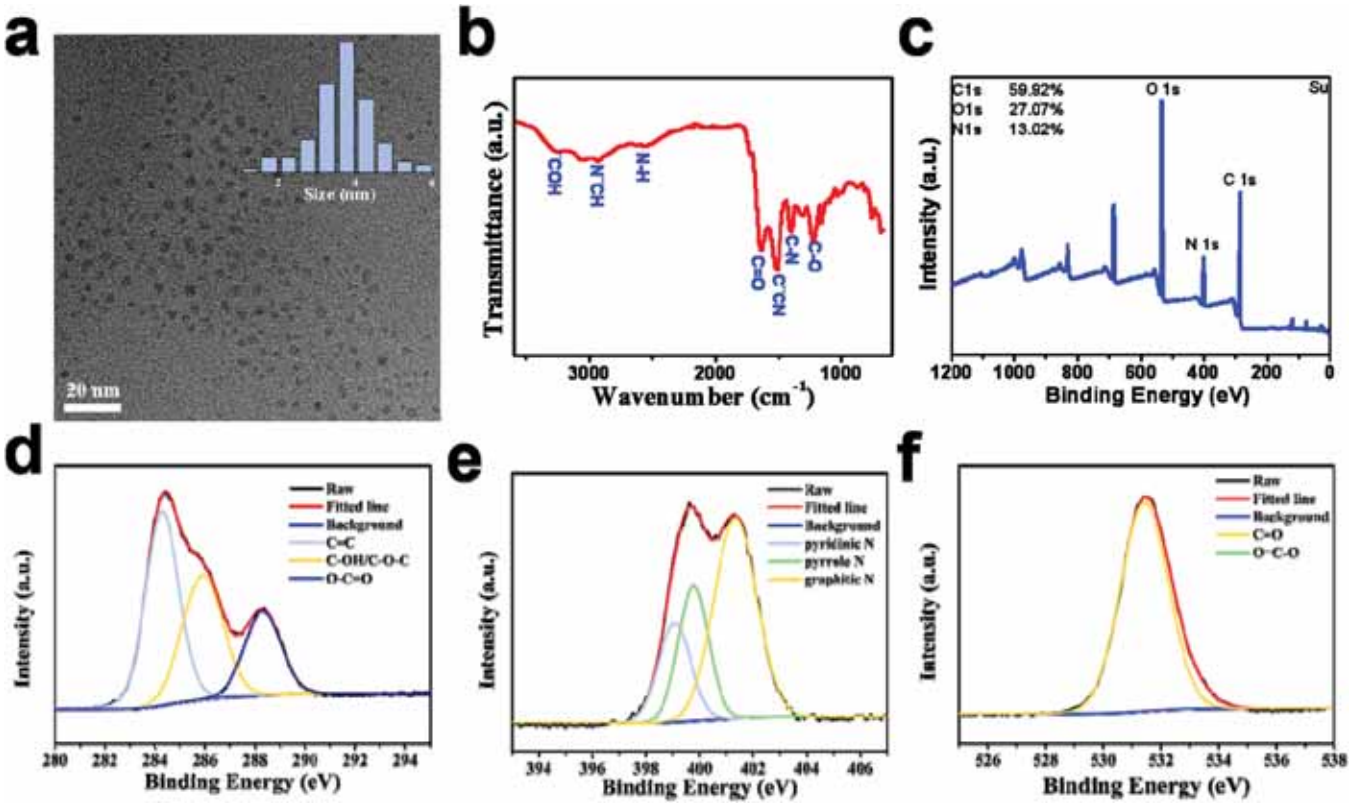

Fig. 1. Structural characterization of the P-CDs (a) TEM image and size distribution of the P-CDs; (b) FT-IR spectra of the P-CDs; (c) XPS spectra; (d) high-resolution $C_{1\,s}$ spectra; (e) high-resolution $N_{1\,s}$ spectra; and (f) high-resolution $O_{1\,s}$ spectra.

CDs targeted on the surface of organelles decreases gradually. Accordingly, the use of fluorescent probes to investigate the process of subcellular structure interaction appears to be insufficiently precise in a specific range. Therefore, there is an urgent need for a method that can target organelles and respond to ions and other substances without diminishing the SBR of the image, so that subcellular structural interactions may be observed more precisely.

STORM uses the photoblinking properties of fluorescent probes to reconstruct a super-resolution image by collecting thousands of photoblinking frames [34–36]. Accordingly, STORM gathers the transient fluorescence signal of the probe, unlike confocal microscopy (CLSM), which collects steady-state fluorescence to capture image information. And STORM does not influence the SBR of the image. Therefore, even if the investigated object quenches the steady-state fluorescence of the probe, the SBR of the STORM image is not impacted so long as the object being measured has a negligible effect on the transient fluorescence of the probe. In other words, when a probe has photoblinking properties, its transient fluorescence had little effect on the response of other substances, and the high SBR can be derived from super-resolution images, which can be used to examine the interaction between the subcellular structure and the image of clear cells. In this study, we designed CDs with photoblinking (P-CDs) properties that can target mitochondria and respond to HS^-. These P-CDs can photoblink without the incorporation of additional compounds, and can still maintain the photoblinking properties while targeting mitochondria and responding to HS^-. Moreover, both in vitro and in vivo investigations demonstrated that the addition of HS^- increased the transient fluorescence of P-CDs without affecting the reconstruction effect. Thus, we acquired super-resolved reconstructed images of HS^--mitochondria interactions with a high SBR, thereby obtaining a novel tool for studying the subcellular structure interactions and revealing the causes of disease.

2. Experimental section

2.1. Chemicals

The P-CDs were synthesized using 3-diethylaminophenol and tartaric acid as the main raw materials, which were purchased from Shanghai Sinopharm Chemical Reagent. In addition, the reagents (NaOH, HCl, NaCl, GSH, Cys and Hcy) used to study the optical stability of the P-CDs, and the metal salts [NaHS, $Na_2H_2PO_2$, $NaHCO_3$, K_2CO_3, $Ni(NO_3)_2{\cdot}6H_2O$, NaF, NaBr, $Pb(NO_3)_2$, $CuSO_4$, $NaSO_3$, KH_2PO_4 and CH_3COONa] used to study their ion-selectivity were purchased from Macklin.

2.2. Instruments

The morphology, chemical structure, and chemical composition of P-CDs were characterized separately using Transmission electron microscopy (TEM, FEI TECNAI G2 F20, USA), Fourier-transform infrared spectroscopy (FT-IR, Nicolet 5700 spectrometer, USA), X-ray photoelectron spectroscopy (XPS, Thermo Fisher ESCALAB 250Xi, USA). In addition, the optical properties, optical stability, and ion-selectivity of the P-CDs were characterized using ultraviolet-visible spectroscopy (UV–vis, UV-2550 Shimadzu, Japan), fluorescence spectroscopy, lifetime and quantum yield (PL, Fluoro Max-4 Horiba, Japan). Moreover, the targeting ability of the P-CDs was verified using a laser-scanning confocal fluorescence microscope (Nikon A1R MP+, Japan). Other features of the P-CDs, including their photoblinking and cell imaging properties, were analyzed using the STORM home-built, Fig. S1[36]).

2.3. Synthesis of P-CDs

The P-CDs were synthesized via a one-step hydrothermal process using 40 mL of ultrapure water, as well as 1.0 g of 3-diethylaminophenol and 1.0 g of tartaric acid as the carbon and nitrogen sources,

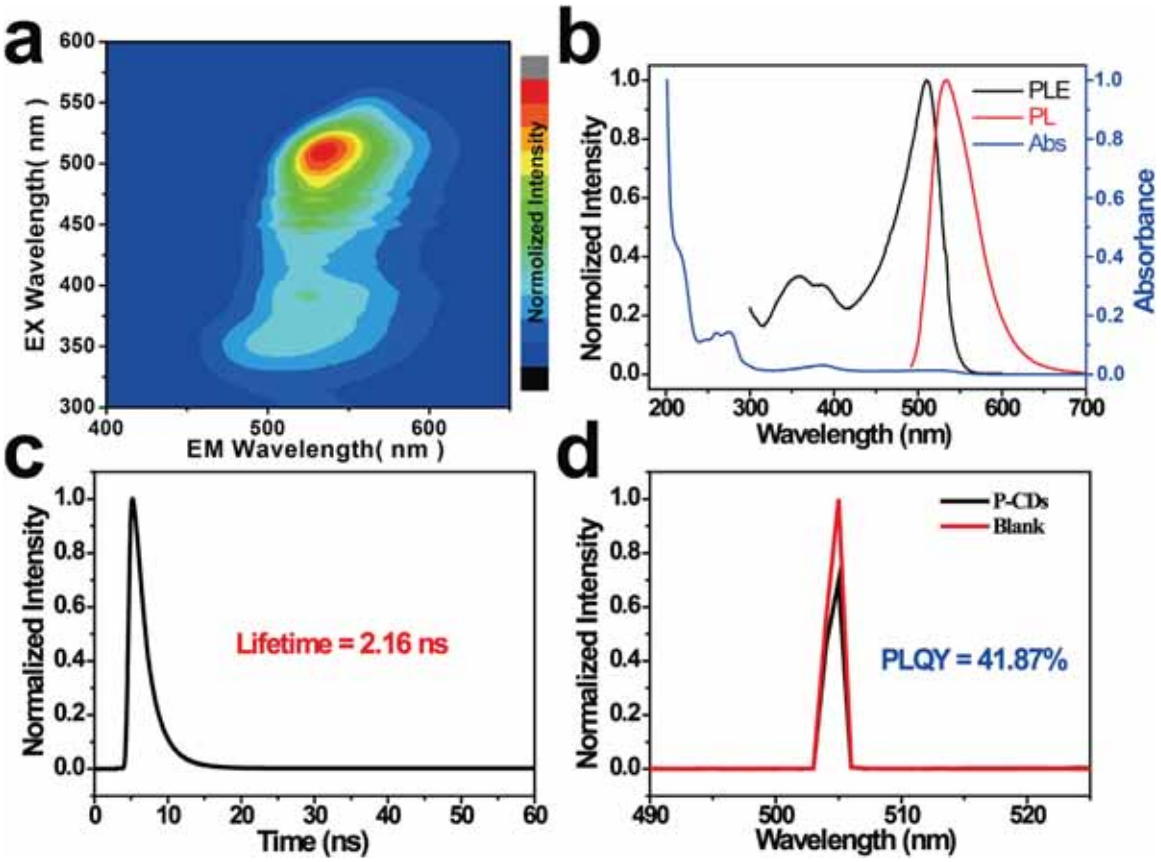

Fig. 2. Optical characterization of the P-CDs (a) The excitation-emission color map with different excitation wavelengths; (b) UV-Vis spectra (blue curve), excitation spectra (black curve), and emission spectra (red curve); (c) fluorescence decay traces and (d) photoluminescence quantum yield.

respectively. The resultant mixture was autoclaved and then placed in a drying cabinet at 180 °C for 18 h. As the solution cooled down to 25 °C, the initial P-CD solution was obtained. This was then transferred to a dialysis membrane (500 Da) to obtain the final P-CD solution after three days of dialysis.

2.4. Specificity and standard curve for the P-CDs-HS$^-$ detection system

P-CD solutions measuring 20 μL, having a concentration of 20 μL/mL, were added into solutions containing HS^-, F^-, Cl^-, Br^-, SO_4^{2-}, CO_3^{2-}, NO_3^-, HCO_3^-, SO_3^{2-}, AC^-, $H_2PO_4^-$, $H_2PO_2^-$, GSH, Cys and Hcy at a 2 mM concentration. Subsequently, changes in the FI of the P-CDs were used to establish the selectivity for these ions.

Additionally, 10 μL of P-CD solutions, having a concentration of 20 μL/mL, were added into solutions containing different concentrations of HS^- (0, 1.0, 2.0, 3.0, 4.0, 5.0, 6.0, 7.0, 8.0, 9.0, 10.0, 15.0, 20.0, 30.0, and 40.0 μM) at 25 ℃. Subsequently, the PL spectra of the P-CDs-HS^- detection system were recorded after 5 mins. The resultant standard curve for the P-CDs-HS^- detection system was based on the "three times the standard deviation" guideline.

2.5. Photoblinking characteristics of the P-CDs

First, different concentrations of P-CD solutions (10, 20 and 30 μL/mL) were added to the object slide, and the sample was placed on STORM's sample stage. Subsequently, 10000 wide-field images of the sample were continually captured in 3 mins. The photoblinking images of P-CDs were obtained by reconstruction. Finally, photoblinking characteristics, such as duty cycle and scintillation lifespan were estimated. Except for the difference in sample preparation [fixed concentrations of P-CDs (10 μL/mL) were added to various concentrations of HS^- solutions (10, 20, 30, 40 and 50 μM)], the photoblinking characteristics of the P-CDs-HS- detection system were identical to those described in the preceding steps.

2.6. Cytotoxicity evaluation of P-CDs

MTT [3-(4,5-dimethylthiazol-2-yl)− 2,5-diphenyl tetrazolium bromide] assay was utilized to investigate the cytotoxicity of P-CDs. HeLa cells were first grown in a 96-well plate and incubated for 24 h in a cell incubator. Various concentrations of the P-CD solutions (blank, 50, 100 and 200 μL/mL) were then added to the 96-well plate, and the plate was incubated for 48 h. Finally, cytotoxicity data for the P-CD solutions were collected. All experiments were repeated more than three times.

2.7. Cellular imaging of P-CDs

The subcellular location of P-CDs was examined using a laser-scanning confocal fluorescence microscope (Nikon A1R MP+). Mito-Tracker@ Deep Red and HeLa cells were co-incubated in the cell incubator for 30 mins. Then, PBS was used to wash the cell culture plate. After three cycles of washing the cells, P-CDs were introduced and held for 10 mins, followed by three PBS washes. Finally, the cell samples were directly observed using a laser-scanning confocal fluorescence microscope.

STORM was utilized to investigate the connections between mitochondrial and HS^-. First, 10 μL of P-CD solutions were added to the cell culture plate and they were incubated in the cell culture chamber for 10 mins. Subsequently, the cell culture plate was rinsed three times with PBS, and HS^- was added. The cell samples were then washed three times in duplicate and then placed on the sample stages of STORM to acquire 10000 wide-field images. Finally, these images were reconstructed to

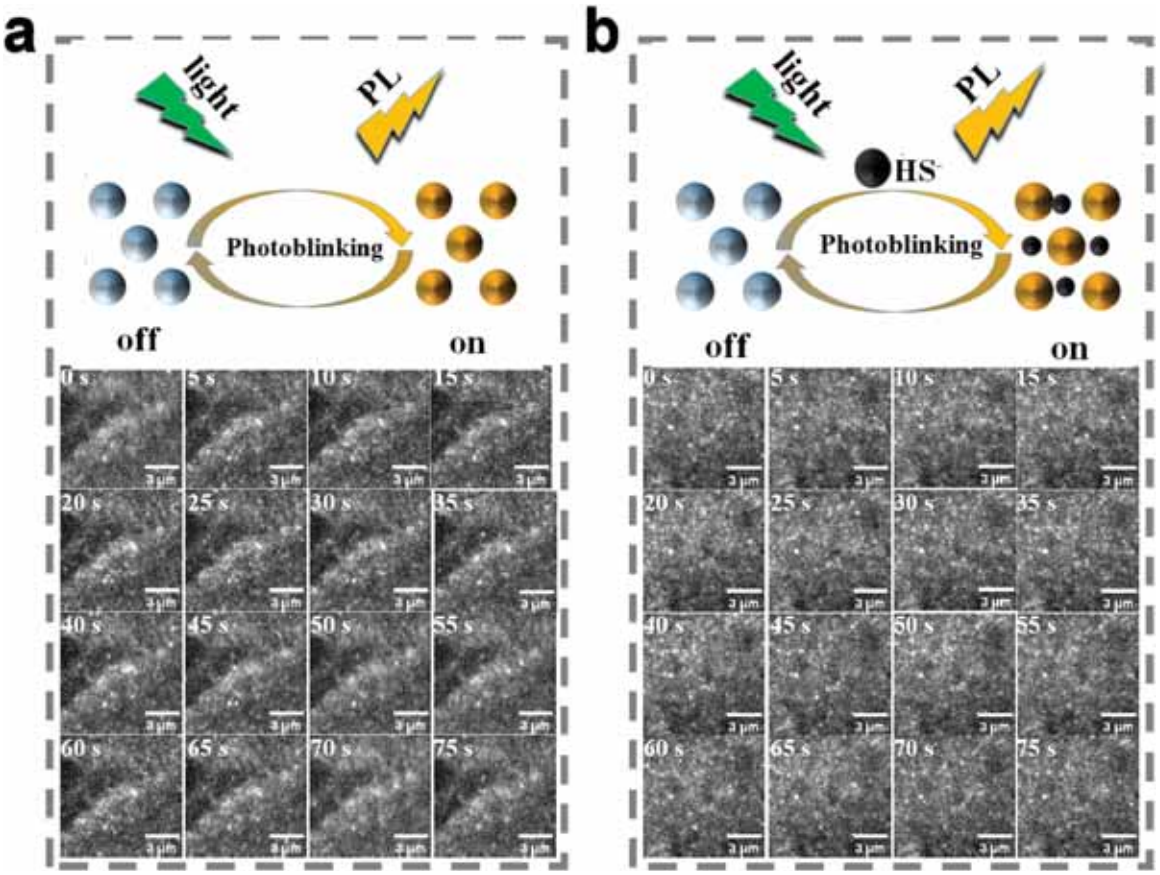

Fig. 3. Photoblinking imaging by STORM: (a) P-CDs and its photoblinking schematic illustration; (a) P-CDs with HS^- (10 μM) and its photoblinking schematic illustration. Scale bar for all images: 3 μm.

obtain super-resolved cells image.

3. Results and discussion

It was essential to take the initiative in carefully defining the structure of P-CD because its structure impacts its optical characteristics and subcellular targeting capabilities. The TEM image and size distribution of the P-CDs demonstrated a uniform dispersion (Fig. 1a). In addition, the P-CD particle sizes varied from 2.5 to 5.5 nm, and the smaller particle size indicated that P-CDs will enter the cell more easily. For the purpose of determining the structure of P-CDs, FT-IR and XPS spectra were systematically examined. Several characteristic bands are visible in the FT-IR spectrum at 3250, 2931, 2551, 1633, 1570, 1391, and 1199 cm^{-1} (Fig. 1b). These bands correspond successively to C-OH (flexural vibrations), N-CH (flexural vibrations), N-H (flexural vibrations), C═O (asymmetric stretching vibrations), C-CH (flexural vibrations), C–N (stretching vibration of the bending modes), and C–O (flexural vibrations) [37]. Additionally, the XPS spectra showed the presence of three peaks (C 1 s, N 1 s, and O 1 s) [38], indicating that the P-CDs were composed of 59.92% C, 13.02% N, and 27.07% O (Fig. 1c). The high-resolution spectra were considerably more beneficial in characterizing the functional groups of P-CDs. Accordingly, three peaks were observed in the high-resolution C 1 s spectrum (Fig. 1d), viz. C═C (284.2 eV), C-O/C-O-C (285.9 eV), and C═O. (288.3 eV). In addition, the N 1 s spectrum of the P-CDs had three distinct N structure types, viz. pyridinic N (399.1 eV), pyrrole N (399.9 eV), and graphitic N (401.3 eV), as depicted in Fig. 1e. Moreover, C═O (531.4 eV) and O═C-O (532.6 eV) were also present in the high-resolution O 1 s spectra (Fig. 1f).

The optical properties of P-CDs are determined by their structure. The 3D excitation-emission spectra of P-CDs are depicted in Fig. 2a, with emission centers at 531–535 nm and excitation centers at 508–513 nm, respectively. Accordingly, the excitation spectra (black curve) and emission spectra (red curve) of the prepared P-CDs were determined to be centered at 510 nm and 534 nm, respectively (Fig. 2b). Additionally, the UV–vis (blue line) spectrum of the P-CDs exhibits two absorption peaks at 268 nm and 386 nm, which have been attributed to the π-π * transition and n-π * transition, respectively [39]. As shown in Figs. 2c and 2d, the average lifetime of P-CDs after the bi-exponential fit was 2.16 ns and the fluorescence quantum yield was 41.87% by direct method. In addition, after identifying the optical properties of the P-CDs, the optical stability was examined as shown in Fig. S2. The variations in FI of the P-CDs with varying concentrations of NaCl (Fig. S2a), time under UV light irradiation (Fig. S2b), and pH (black line in Fig. S2c) were explored, and the results demonstrated that the P-CDs have excellent optical stability. Meanwhile, variations in the FI of P-CDs-HS^- with varying pH (red line in Fig. S2c) and the response time of P-CDs-HS^- were also investigated (Fig. S2d), confirming their good stability and short response time. Moreover, the high selectivity and anti-interference capacity of the P-CDs to HS^- is also demonstrated in the selectivity (Fig. S3a) and anti-interference (Fig. S3b) experiments. Additionally, P-CDs for HS^- detection were found to possess a broad detection range (2–50 μM , Fig. S3c) and a low detection limit as 62.24 nM (Fig. S3d). As shown in Table S1, compared with other fluorescent probes reported previously for HS^- detection, the P-CDs has a lower detection limit and similar linear range. To understand the mechanism of the P-CDs targeting mitochondria and the mechanism of HS^- quenching, the Zeta potential were measured of P-CDs and their addition to HS^- (Fig S4). The zeta potential of P-CDs is + 6.2 mV, indicating they can target mitochondria by electrostatic attraction [29]. The zeta potential of P-CDs-HS^- is + 1.0 mV, it is shown that P-CDs are attracted to HS^- by electrostatic interaction. At the same time, it can be seen from the Fig

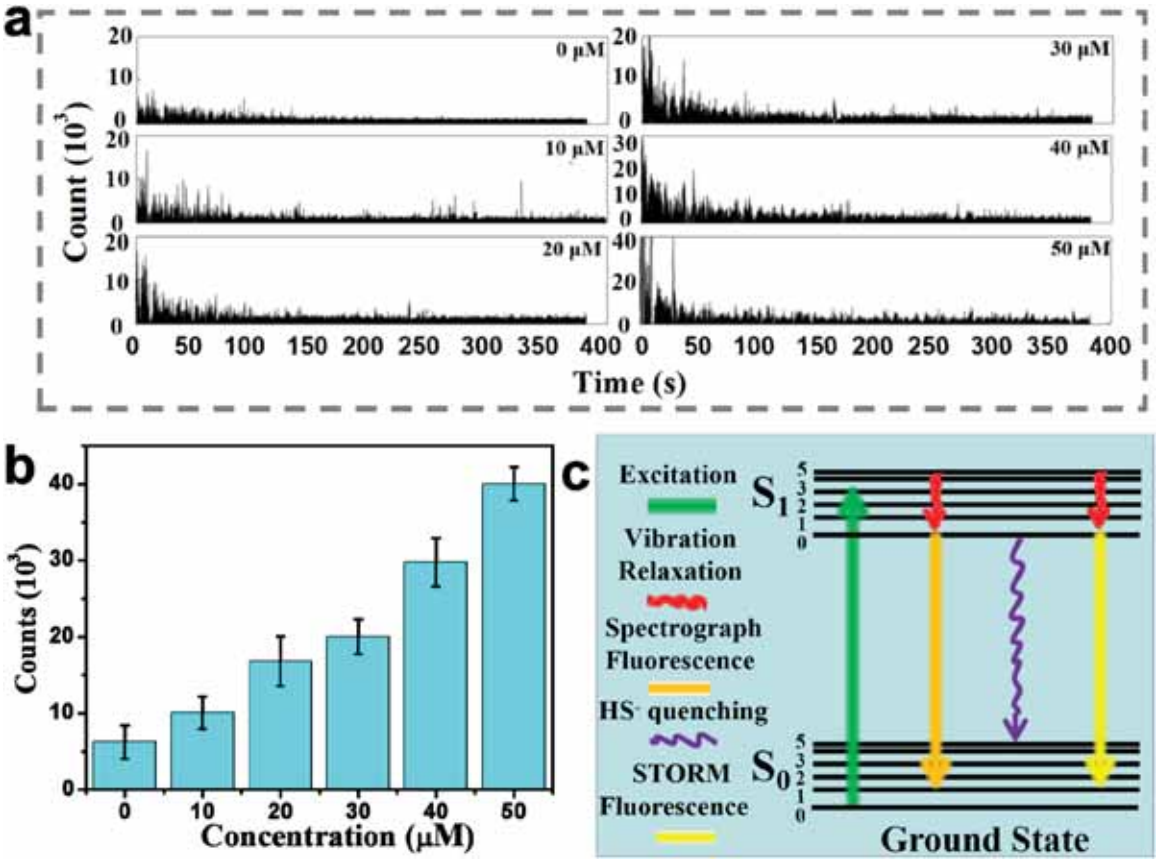

Fig. 4. (a) Fluorescence time traces of P-CDs with different concentrations of the HS^- solutions (0, 10, 20, 30, 40, and 50 μM); (b) Instantaneous maximum photons of P-CDs with different concentrations of HS^- solutions (0, 10, 20, 30, 40, and 50 μM); (c) Energy-level diagram of P-CDs in different situations.

S3c that the fluorescence emission center of P-CDs did' t change with HS^- addition. So, it can be considered that the quenching is dependent on the PET mechanism.

According to the aforementioned studies, P-CDs exhibit excellent stability, high sensitivity, quick response time, and good selectivity for HS^- response, making them an excellent probe for detecting HS^-. Prior to application to STORM, however, it must be verified if the probe has photoblinking properties. Accordingly, the photoblinking of P-CDs was investigated using STORM. A total of 48000 photoblinking frames of the P-CDs were captured at a power of 1 kW/cm^2 and a rate of 60 frames per second (Fig. 3a and Supporting Information Video 1). Accordingly, the photoblinking capability of the P-CDs was directly confirmed. In addition, it was determined whether the photoblinking of P-CDs-HS^- was a fundamental requirement for STORM, in order to analyze the interaction between HS^- and subcellular structures. Accordingly, STORM-based images of the P-CDs with HS^- (10 μM) were collected under identical shooting conditions. Moreover, it was also proved that the addition of ions does not eliminate the photoblinking phenomenon of P-CDs (Fig. 3b and Supporting Information Video 2). The whole process of photoblinking P-CDs in smaller field of view is shown in the Video 3, which further proves the photoblinking characteristics of P-CDs.

Supplementary material related to this article can be found online at doi:10.1016/j.snb.2023.133434.

After discovering that P-CDs exhibit photoblinking and that HS^- has no effect on photoblinking, the transient optical characteristics of P-CDs were systematically examined. On a clean glass coverslip, diluted P-CD solutions with varying concentrations of HS^- solutions were dripped to form a thin layer of the specimen, which was then analyzed using the STORM image system. As shown in Fig. 4a, the photoblinking of P-CDs at various concentrations of HS^- solutions can be detected. In addition, statistics on the instantaneous maximum photons of P-CDs reveal that the number of photons grows as HS^- concentration changes (Fig. 4b). This was the exact opposite of the trend of FI change, following the use of PL for P-CDs in response to varying concentrations of the HS^- solutions. Consequently, an examination of this phenomenon was required. As illustrated in Fig. 4c, the P-CDs were excited by the excitation light (green arrow) and their energy level jumped from S_0 to S_1; after the vibration relaxation, an S_1 to S_0 level jump and fluorescence (orange arrow) was seen (red arrow). The fluorescence is quenched after the addition of HS^- and P-CDs (purple arrow), as determined by the PI measurement of the fluorescence intensity (FI). However, when STORM is utilized to identify the FI of P-CDs with HS^-, the fluorescence may be plainly noticed and its FI was significantly enhanced (yellow arrow). Accordingly, the mechanistic explanation was depicted in Fig. S5. The FI of P-CDs was affected by aggregation quenching and the addition of HS^-. Although the effect of aggregation quenching on P-CDs was reduced, the number of P-CDs that can generate fluorescence was also reduced, resulting in a decrease in the average fluorescence intensity of P-CD solutions observed by PI. In contrast, STORM capitalizes on the reduction in the effect of aggregation quenching of P-CDs after the addition of HS^- to capture the transient fluorescence of individual P-CDs, allowing for the observation of stronger fluorescence signals.

To evaluate the effect of STORM probe, the duty cycle and fluorescence-on time of the fluorescent probe were also required. The duty cycle curve plateaued after 220 s (Fig. 5a), and statistics on the duty cycle of P-CDs revealed that the value varies with HS^- concentration (Fig. 5b). This facilitates the reconstruction of an image from a small number of raw frames with an enhanced temporal resolution. In addition, the average "on" time of fluorescence for P-CDs with varying concentrations of HS^- solutions was calculated to be 81.20, 70.52, 99.21, 101.23, 124.4, and 134.01 ms, respectively. Accordingly, it provides a reference for camera sampling frequency. Thus, in light of the

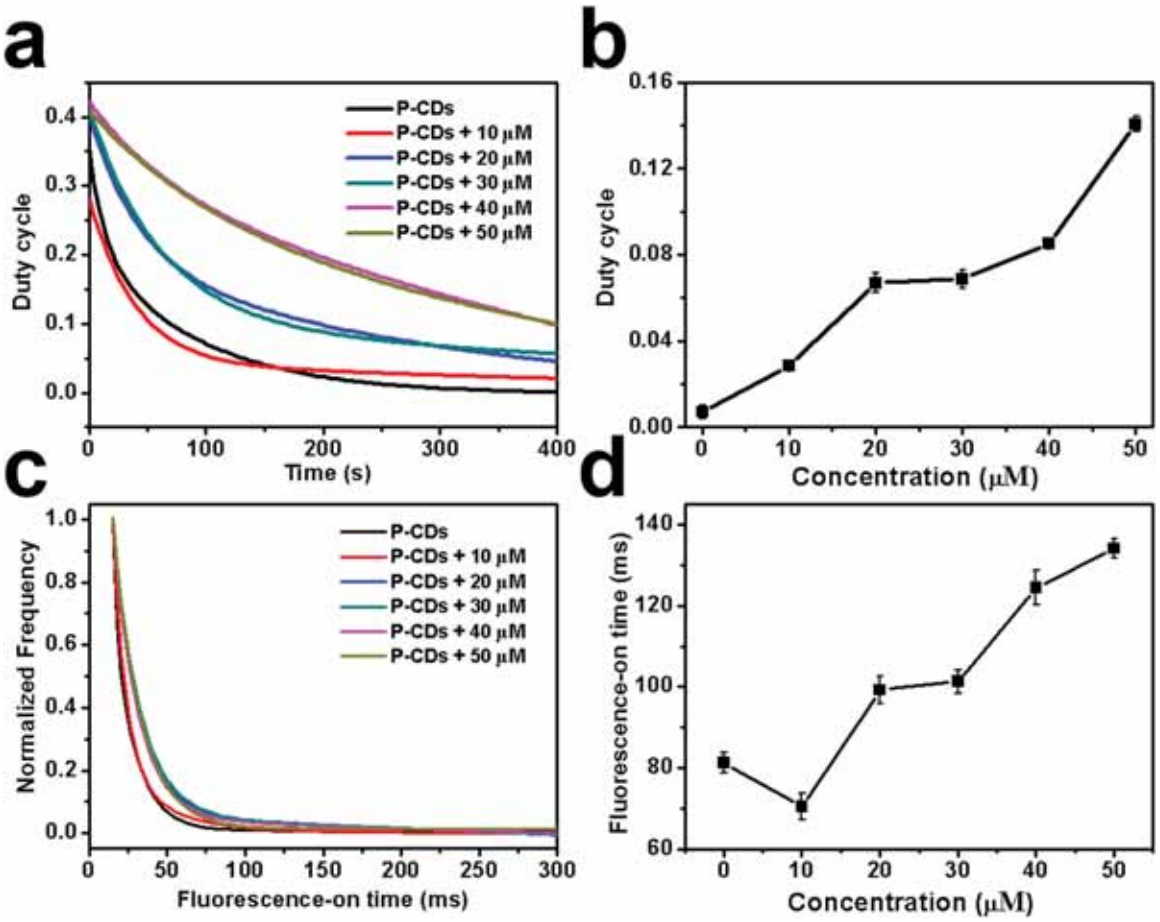

Fig. 5. Photoblinking properties of the P-CDs with different concentrations of the HS^- solutions (0, 10, 20, 30, 40, and 50 μM)): (a) On-off duty cycle and the survival fraction plot vs time; (b) On-off duty cycle after calculation; (c) Distribution of the "on" times (λ_{ex} = 543 nm) at a laser power density of 1 kW·cm^{-2}; (d) Fluorescence-on time after calculation.

aforementioned photoblinking characteristic of P-CDs, the feasibility of STORM imaging in living cells was adequately demonstrated.

Before employing P-CDs as a probe for STORM imaging of living cells, it was crucial to examine their cytotoxicity and targeting capability. Accordingly, MTT (Fig. 6a) assay was used to examine the cytotoxicity of the P-CDs, and it was found that the HeLa cells maintain good cell viability when the P-CDs concentration increases. In addition, the coefficient was determined from the living cell CLSM imaging (Figs. 6b, 6c, and 6d) of the P-CDs that were co-localized with MitoTracker@Deep Red and was found to be as high as 0.934 (Fig. 6e). Since MitoTracker@Deep Red had been shown to target mitochondria previously, and due to the fact that the target position of P-CDs coincides with its high coefficient, P-CDs were confirmed to have an exceptional ability to target mitochondria. Moreover, after labeling live cells, some probes lose their photoblinking properties, rendering them incompatible with the STORM imaging system; hence, the photoblinking effect of P-CDs added to live cells must be studied. A total of 10000 STROM-based living cells images of the P-CDs were collected at a power of 1 KW/cm^2 and at a frequency of 60 frames per second (Fig. 6b). Thus, it was directly demonstrated that P-CDs in living cells possess photoblinking properties.

The aforementioned findings indicate that P-CDs were ideally suited for investigating mitochondrion-HS^- interactions using the STORM imaging system. In Fig. 7a, bright mitochondrial structures can be detected in the wide-field image. However, the mitochondrial structure is more apparent in the STORM image in comparison to the wide-field image, although the W-S splicing images provided a clearer view. In addition, resolution calculations were performed for structures common (yellow bar of image) to the wide-field and STORM image; correspondingly, the resolution in the wide field was found to be 225.1 nm, whereas, the resolution in the STORM was 103.3 nm. Accordingly, the imaging resolution was more than doubled (Fig. 7c). The improved resolution aided in a better understanding of the interaction between the subcellular structures. As shown in Fig. 7b, HS^- (10 μM) was added to live cells incubated with P-CDs, and the FI was significantly quenched. Additionally, the SBR was lowered in wide-field images, making it impossible to see any structure in living cells. However, the SBR in STORM images did not change significantly (Fig. 7d). Thus, it was still possible to observe the super-resolved structure of mitochondria in living cells. Therefore, when using STORM to research HS^--mitochondria interactions, images with a greater SBR can be obtained in addition to super-resolution images, allowing the interaction to be analyzed more clearly and precisely.

4. Conclusion

In conclusion, photoblinking P-CDs were synthesized using a facile hydrothermal approach. Through a series of investigations, it was determined that P-CDs had excellent stability, strong selectivity for HS^- response, high sensitivity, and a response time, allowing it to be utilized as a probe with superior HS^- detection capability. In addition, the excellent photoblinking characteristics of the P-CDs were confirmed, and it was determined that the P-CDs meet all requirements for use as a probe in the STORM imaging system. Moreover, P-CDs exhibited low cytotoxicity and excellent targeting capability for mitochondria; hence, it may also be employed as a fluorescent probe for targeting

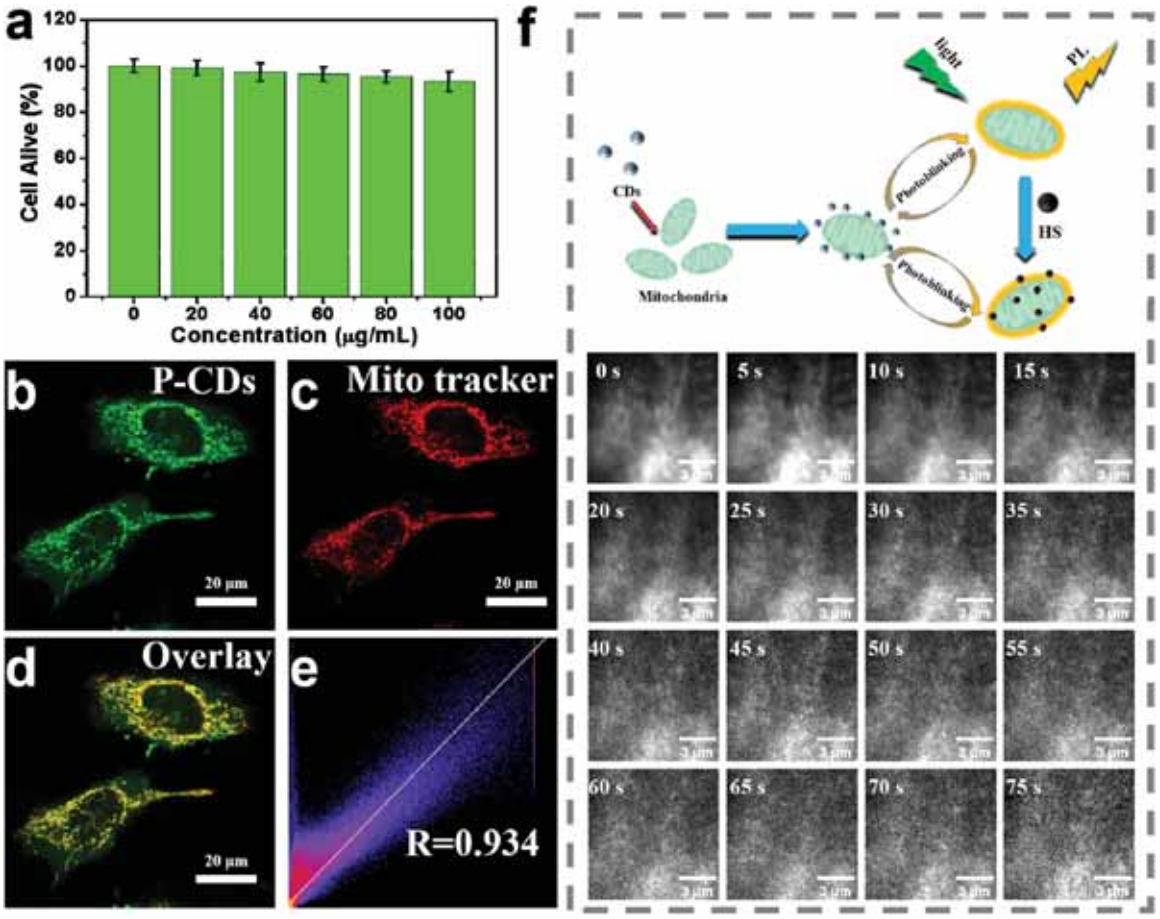

Fig. 6. Cytotoxicity, subcellular co-localization assays, and photoblinking imaging of the P-CDs in living cells: (a) Cytotoxicity of the different P-CD concentrations; CLSM images of living HeLa cells treated with: (b) P-CDs (excitation wavelength: 488 nm); (c) MitoTracker@Deep Red (excitation wavelength: 644 nm; (d) P-CDs and MitoTracker@Deep Red overlay; (e) calculated coefficients in Fig. 6(d); (f) photoblinking imaging of P-CDs and its photoblinking schematic diagram in living cells (scale bar: 3 μm).

mitochondria in living cells. Lastly, in conjunction with the preceding investigations, the interaction between HS^- and mitochondria was investigated using the STORM imaging system with P-CDs as fluorescent probes. Accordingly, super-resolution images were obtained, which more than doubled the resolution of wide-field imaging to 103.3 nm. Simultaneously, pictures with a high signal-to-background ratio were produced, enabling the interaction between HS^- and mitochondria to be observed in detail. As a visualization method, the aforementioned method effectively eliminates the influence of the signal-to-background ratio reduction on the image definition after fluorescence quenching, and at the same time, higher-resolution images can be obtained, allowing the interaction between subcellular structures to be studied more clearly and precisely, and the causes of related diseases to be uncovered.

Compliance with ethical standards

none.

CRediT authorship contribution statement

Conceptualization: **Jiaqing Guo**, **Jinying Wang**, **Hao Li**. Methodology: **Jiaqing Guo**, **Aikun Liu**. Validation: **Jiaqing Guo**, **Aikun Liu**. Formal analysis: **Jiaqing Guo**, **Jinying Wang**, **Hao Li**. Investigation: **Jiaqing Guo**, **Yejun He**. Writing - original draft: **Jiaqing Guo**, **Jinying Wang**, **Hao Li**. Writing - review & editing: **Jiaqing Guo**, **Jinying Wang**, **Hao Li**, **Zhigang Yang**, **Jun Song**. Resources: **Yejun He**, **Zhigang Yang**. Funding acquisition: **Jiaqing Guo**, **Hao Li**, **Zhigang Yang**, **Jun Song**, **Junle Qu**,

Declaration of Competing Interest

The authors declare that they have no known competing financial interests or personal relationships that could have appeared to influence the work reported in this paper.

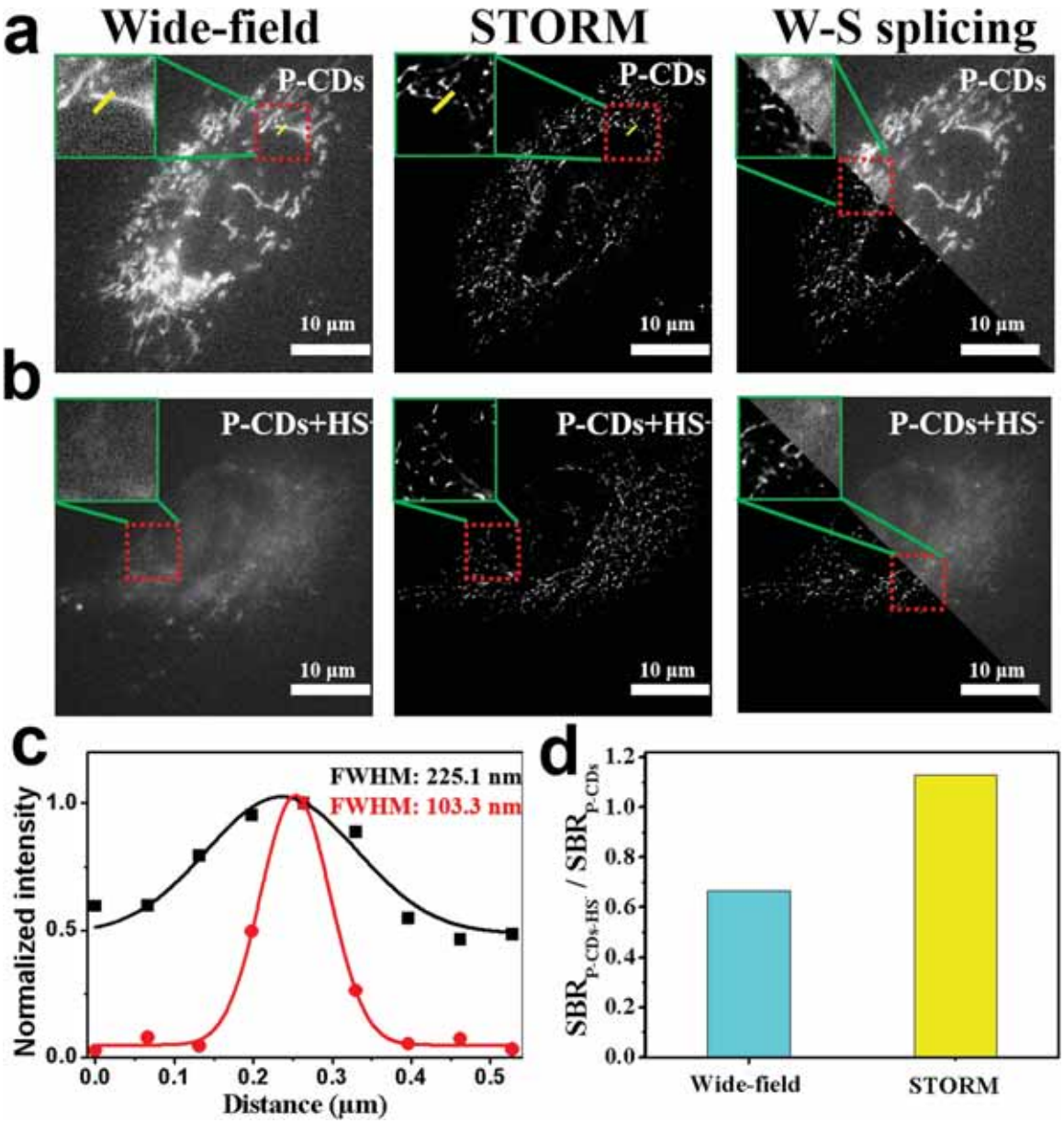

Fig. 7. Wide-field and STORM imaging of live HeLa cells using P-CDs (a) Wide-field, STORM, and splicing image of the P-CDs, inset: Red areas show images; (a) Wide-field, STORM, and splicing image of the P-CDs with HS^- (10 μM), inset: Red areas show images; (c) highlighted in Fig. 7(a) yellow bar, fit to Gaussian equations with the FWHM values; (d) SBR of Wide-field and STORM imaging by P-CDs and P-CDs with HS^- (10 μM). Scale bar for all images: 10 μm.

Data availability

Data will be made available on request.

Acknowledgments

This work has been partially supported by the National Key R&D Program of China (2021YFF0502901), National Natural Science Foundation of China (62175161/61835009/62127819/61875131/62071306/61975127), China Postdoctoral Science Foundation (2021M702240), Shenzhen Basic Research Program (JCYJ20210324095810028/ JCYJ20210324095613036).

Appendix A. Supporting information

Supplementary data associated with this article can be found in the online version at doi:10.1016/j.snb.2023.133434.

References

[1] P. Gao, W. Pan, N. Li, B. Tang, Fluorescent probes for organelle-targeted bioactive species imaging, Chem. Sci. 10 (2019) 6035.
[2] H.M. Kim, B.R. Cho, Small-molecule two-photon probes for bioimaging applications, Chem. Rev. 115 (2015) 5014–5055.
[3] S.M. Feng, J.R. Zheng, J.Z. Zhang, et al., Fe^{2+} imaging in ferroptosis and drug-induced liver injury with a ratiometric near-infrared fluorescent probe, Sens. Actuators B: Chem. 15 (2022), 132512.
[4] S. Chen, Jy Fan, My Lv, et al., Internal standard assisted surface-enhanced raman scattering nanoprobe with 4-NTP as recognition unit for ratiometric imaging hydrogen sulfide in living cells, Anal. Chem. 94 (2022) 14675–14681.
[5] H. Shaath, A. Vishnubalaji, Y. Elkord, et al., Single-cell transcriptome analysis highlights a role for neutrophils and inflammatory macrophages in the pathogenesis of severe COVID-19, Cells 9 (2020) 2374.
[6] R. Sanjay, T. Benzouak, S. Gunpat, et al., Fatigue symptoms associated with COVID-19 in convalescent or recovered COVID-19 patients; a systematic review and meta-analysis, Ann. Behav. Med. 3 (2022) 219–234.
[7] J. Zielonka, J. Joseph, A. Sikora, et al., Mitochondria-targeted triphenylphosphonium-based compounds: syntheses, mechanisms of action, and therapeutic and diagnostic applications, Chem. Rev. 117 (2017) 10043–10120.

[8] K. Qiu, Y. Chen, T.W. Rees, et al., Chemically engineered mesoporous silica nanoparticles based intelligent delivery systems for theranostic applications in multiple cancerous/non-cancerous diseases, Coord. Chem. Rev. 378 (2019) 66–86.
[9] Lee Mh, Kim Js, Sessler Jl, Small molecule-based ratiometric fluorescence probes for cations, anions, and biomolecules, Chem. Soc. Rev. 44 (2015) 4185–4191.
[10] W.Q. Lai, J.Q. Guo, N. Zheng, et al., Selective determination of 2,4,6-trinitrophenol by using a novel carbon nanoparticle as a fluorescent probe in real sample, Anal. Bioanal. Chem. 412 (2020) 3083–3090.
[11] Z. Wu, W. Li, J. Chen, et al., A graphene quantum dot-based method for the highly sensitive and selective fluorescence turn on detection of biothiols, Talanta 119 (2014) 538–543.
[12] Y. Yan, J. Gong, J. Chen, et al., Recent advances on graphene quantum dots: from chemistry and physics to applications, Adv. Materials 31 (2019) 1808283.
[13] K. Jiang, Y. Wang, X. Gao, et al., Facile, quick, and gram-scale synthesis of ultralong-lifetime room-temperaturephosphorescent carbon dots by microwave irradiation, Angew. Chem. Int. Ed. 57 (2018) 6216–6220.
[14] M.L. Liu, B.B. Chen, C.M. Li, et al., Carbon dots: synthesis, formation mechanism, fluorescence origin and sensing applications, Green. Chem. 21 (2019) 449–471.
[15] Z. Zhang, G. Yi, P. Li, et al., A minireview on doped carbon dots for photocatalytic and electrocatalytic applications, Nanoscale 12 (2020) 13899–13906.
[16] W.P. Ma, X.P. Quan, B. Yan, A dual-emission Eu(III) functionalized multi-ligand MOFs for wide range pH sensing, Dyes Pigments 206 (2022), 110648.
[17] Y.M. Zhang, Y.C. Chen, Fang Hb, et al., A ratiometric pH probe for acidification tracking in dysfunctional mitochondria and tumour tissue in vivo, J. Mater. Chem. B 10 (2022) 5422–5429.
[18] M.L. Li, Y. Huang, S.M. Song, et al., Piperazine-based mitochondria-immobilized ph fluorescent probe for imaging endogenous $ONOO^-$ and real-time tracking of mitophagy, ACS Appl. Bio Mater. 5 (2022) 2777–2785.
[19] Q.Q. Bai, C.J. Yang, M.J. Yang, et al., pH-dominated selective imaging of lipid droplets and mitochondria via a polarity-reversible ratiometric fluorescent probe, Anal. Chem. 94 (2022) 2901–2911.
[20] B. Luo, K.Y. Liu, Y.L. Chen, et al., Construction of a rational-designed multifunctional platform based on a fluorescence resonance energy transfer process for simultaneous detection of pH and endogenous peroxynitrite, Anal. Chem. 93 (2021) 9064–9073.
[21] W.J. Xu, P. Wu, X.X. Li, et al., Two birds with one stone: a highly sensitive near-infrared BODIPY-based fluorescent probe for the simultaneous detection of Fe^{2+} and H^+ in vivo, Talanta 233 (2021), 122601.
[22] J.T. Hou, B.Y. Wang, P.W. Fan, et al., A novel benzothiazine-fused coumarin derivative for sensing hypochlorite with high performance, Dyes Pigments 182 (2020), 108675.
[23] X.P. Pang, L. Li, P.Y. Wang, et al., Adenine-derived carbon dots for the chemosensing of hypochlorite based on fluorescence enhancement, Microchem. J. 168 (2021), 106400.
[24] I.M. Resta, B. Bedrina, E. Martinez, et al., Detection of subcellular nitric oxide in mitochondria using a pyrylium probe: assays in cell cultures and peripheral blood, J. Mater. Chenistry B 9 (2021) 9885–9892.
[25] Y.J. Nie, S.H. Wang, Y.X. Lin, et al., Highly sensitive fluorescent probe for selective detection of hypochlorite ions using nitrogen-fluorine co-doped carbon nanodots, Spectrochim. Acta Part A-Mol. Biomol. Spectrosc. 250 (2021), 119231.
[26] Z.P. Liu, Q. Sun, M. Yan, et al., Activity-based fluorescent molecular logic gate probe for dynamic tracking of mitophagy induced by oxidative stress, Anal. Chem. 7 (2021) 3502–3509.
[27] L.F. Guo, H. Liu, X. Jin, et al., Development of reaction-free and mitochondrion-immobilized fluorescent probe for monitoring pH change, Sens. Actuators B: Chem. 341 (2021), 129962.
[28] R.T. Ágata, A.Z. Edurne, G.G. Fernando, et al., Mitochondria selective trackers for long-term imaging based on readily accessible neutral BODIPYs, Chem. Commun. 57 (2021) 5318–5321.
[29] H.J. Cai, A.K. Liu, Y.T. Zeng, et al., Multifunctional nitrogen-doped carbon dots for HS^- sensing and mitochondrial-targeted imaging, Sens. Actuators B: Chem. 367 (2022), 132048.
[30] G. Gao, Y.W. Jiang, J.J. Yang, et al., Mitochondria-targetable carbon quantum dots for differentiating cancerous cells from normal cells, Nanoscale 46 (2017) 18368–18378.
[31] X.W. Hua, Y.W. Bao, Z. Chen, et al., Carbon quantum dots with intrinsic mitochondrial targeting ability for mitochondria-based theranostics, Nanoscale 30 (2017) 10948–10960.
[32] P.L. Gao, J.W. Wang, M. Zheng, et al., Lysosome targeting carbon dots-based fluorescent probe for monitoring pH changes in vitro and in vivo, Chem. Eng. J. 381 (2020), 122665.
[33] Q.L. Wang, L.H. Shi, J.H. Zhao, et al., Fluorescent carbon dots with real-time nucleolus-monitoring capability for gene delivery and biosensing of NO_2^- and pH, Appl. Surf. Sci. 599 (2022), 153902.
[34] M. Gao, F. Yu, C. Lv, et al., Fluorescent chemical probes for accurate tumor diagnosis and targeting therapy, Chem. Soc. Rev. 46 (2017) 2237–2271.
[35] Z.G. Yang, J.H. Lee, H.M. Jeon, et al., Folate-based near-infrared fluorescent theranostic gemcitabine delivery, J. Am. Chem. Soc. 135 (2013) 11657–11662.
[36] W. Li, W.H. Pan, M.N. Huang, et al., Disulfide-reduction-triggered spontaneous photoblinking Cy5 probe for nanoscopic imaging of mitochondrial dynamics in live cells, Anal. Chem. 93 (2021) 2596–2602.
[37] H. Wang, M.L. Zhang, K.Q. Wei, et al., Pyrrolic nitrogen dominated the carbon dot mimic oxidase activity, Carbon 179 (2021) 692–700.
[38] H. Li, H.B. Wang, J.Q. Guo, et al., Long-wavelength excitation of carbon dots as the probe for real-time imaging of the living-cell cycle process, Sens. Actuators B: Chem. 311 (2020), 127891.
[39] L. Jiang, H.H. Ding, Xu Ms, et al., UV-Vis-NIR Full-Range Responsive Carbon Dots with Large Multiphoton Absorption Cross Sections and Deep-Red Fluorescence at Nucleoli and In Vivo, Small 16 (2020) 2000680.

Jiaqing Guo was born in Shanxi，China, in 1992. He received the B.S. and the M.S. degree from Minnan Normal University, Fujian, China, in 2015 and 2018, and the Ph.D. degrees from Shenzhen University, Shenzhen, China, in 2021. Since 2021, he has been a Post-doctor at Shenzhen University, Shenzhen, China.

Jinying Wang was born in Jilin, China, in 1999. She received the B.S. degree from Changchun Science and Engineering University, Changchun, China, in 2020. Since September 2020, she has been a master at Shenzhen University, Shenzhen, China.

Aikun Liu was born in Shandong, China, in 1993. She received the B.S. degree from Taishan Medical University, Shandong province, China, in 2016. And the M.S. degrees from Shandong First Medical University, Shandong province, China, in 2019, respectively. Since 2019, she has been a Ph.D at Shenzhen University, Shenzhen, China.

Hao Li was born in Jilin, China, in 1985. He received the B.S. and the M.S. degree from Changchun Science and Engineering University, Changchun, China, in 2008 and 2011, and the Ph.D. degrees from Soochow University, Suzhou, China, in 2016. Since 2020, he has been a associate researcher at Shenzhen University, Shenzhen, China. His research interests include preparation of carbon dots and their application in bioimaging and optoelectronic devices.

Yejun He received the Ph.D. degree in information and communication engineering from the Huazhong University of Science and Technology, Wuhan, China, in 2005. From 2005–2006, he was a Research Associate with the Department of Electronic and Information Engineering, Hong Kong Polytechnic University, Hong Kong. From 2006–2007, he was a Research Associate with the Department of Electronic Engineering, Faculty of Engineering, the Chinese University of Hong Kong, Hong Kong. In 2012, he was a Visiting Professor with the Department of Electrical and Computer Engineering, University of Waterloo, Waterloo, ON, Canada. From 2013–2015, he was an Advanced Visiting Scholar (Visiting Professor) with the School of Electrical and Computer Engineering, Georgia Institute of Technology, Atlanta, GA, USA. Since 2011, he has been a Full Professor with the College of Electronics and Information Engineering, Shenzhen University.

Junle Qu was born in Shanxi, China, in 1970. He received the B.S. degree from Xi' an Jiao Tong University, Xi' an, China, in 1992, and the Ph.D. degree from the Xi' an Institute of Optics and Fine Mechanics, Chinese Academy of Sciences, Beijing, China, in 1998, respectively. Since 2003, he has been a Professor with the Institute of Optoelectronics, Shenzhen University, Shenzhen, China. His research interests include nanophotonics, biophotonics, microscopic imaging technique, and laser treatment technology.

Zhigang Yang was born in Hubei province, China, in September 1981. He received the BS. degree in Chemical Engineering from China University of Geoscience (Wuhan), Hubei, China, in 2004, and the Ph.D. degree from Dalian University of Technology, Dalian, China, in 2011. Since 2017, he has been an associate professor with the Institute of Optoelectronics, Shenzhen University, Shenzhen, China. His research interests focus on optical probe and its applications in biomedical imaging and diagnosis, super-resolution imaging, etc.

Jun Song was born in Inner Mongolia, China, in August 1978. He received the B. Eng. degree in information engineering from Zhejiang University, Zhejiang, China, in 2001, and the Ph.D. degree from Zhejiang University, Hangzhou, China, in 2006. Since 2017, he has been a professor with the Institute of Optoelectronics, Shenzhen University, Shenzhen, China. His research interests include nanophotonics and its applications in renewable energy, biomedicine, electronic information, and environmental protection.